Effects of detailed charge exchange interactions in DSMC-PIC simulation of a simplified plasma test cell

IEPC-2011-112

Presented at the 32nd International Electric Propulsion Conference,
Wiesbaden, Germany
September 11–15, 2011

Paul N. Giuliano* and Iain D. Boyd†
Nonequilibrium Gas and Plasma Dynamics Laboratory, University of Michigan, Ann Arbor, MI, 48109, USA

Abstract: This study concerns the validation of heavy species interaction models commonly used in simulations of Hall effect thrusters. A comparison is made of ion-beam scattering simulations using isotropic and anisotropic scattering models with experimental data from a simplified plasma test cell. The simulation technique utilized is a hybrid DSMC-PIC method which represents heavy species as particles and electrons as a Boltzmann-like fluid. Momentum exchange and charge exchange interactions are the first step in an incremental plan to ultimately simulate collective effects kinetically in low-temperature, magnetized plasma devices such as Hall effect thrusters. The addition and refinement of a more realistic anisotropic scattering model, utilizing a differential cross-section algorithm, shows the best agreement between simulated current collected on the walls of the test cell and experimentally gathered data. In addition, a need to fully resolve the effects of secondary electron emission for a simulation of this type is discussed.

Nomenclature

A_{el}	= First cross-section curve-fitting coefficient for momentum-exchange interactions
A_{ct}	= First cross-section curve-fitting coefficient for charge-exchange interactions
B_{el}	= Second cross-section curve-fitting coefficient for momentum-exchange interactions
B_{ct}	= Second cross-section curve-fitting coefficient for charge-exchange interactions
d	= Atomic diameter
g	= Relative velocity
Kn	= Knudsen number
ω	= Viscosity temperature coefficient
θ_{el}	= Cross-section curve-fitting limit of integration for momentum-exchange interactions
θ_{ct}	= Cross-section curve-fitting limit of integration for charge-exchange interactions
θ	= Post-collision scattering angle
$\sigma_{\text{CEX,MEX}}$	= Collision cross-section
$\frac{d\sigma}{d\Omega}$	= Differential collision cross-section
T	= Temperature
γ	= Secondary electron emission coefficient
Γ	= Incident flux due to heavy species or electrons

*Ph.D. Candidate, Department of Aerospace Engineering, pgiulian@umich.edu.
†James E. Knott Professor of Engineering, Department of Aerospace Engineering, iainboyd@umich.edu.

I. Introduction

This study concerns an electric propulsion modeling effort with a focus on stepping back from full-device Hall effect thruster (HET) modeling in order to validate tools which can simulate and predict the fundamental physical processes occurring in HET operation. There is a particular interest in the simulation of anomalous electron transport mechanisms through the use of kinetic methods such as direct simulation Monte Carlo (DSMC) and particle-in-cell (PIC) algorithms. Kinetic methods have the advantage of not limiting electron behavior to fluid assumptions, such as having a Maxwellian distribution, which have been proven to be grossly inaccurate due to such nonequilibrium phenomena as inelastic processes and sheath formation.

However, it is largely understood that anomalous electron transport is a collective effect arising in magnetized, low-temperature devices such as HETs, requiring high fidelity simulation of more than just electron physics. The inelastic processes and transport mechanisms of the heavy species involved in these devices must be understood so that an anomalous transport model can be built incrementally, introducing the complexities of multiple species, device geometry, and magnetic fields. The aim of this computational study is to mirror the developments of an experimental counterpart in which a high-voltage xenon ion beam is accelerated into a controlled test cell for the purpose of observing the physics of momentum- and charge-exchange scattering effects. This study utilizes the kinetic simulation tool MONACO-PIC (MPIC) to compare simulated ion-beam environments to experimental values via a juxtaposition of cross-section and post-collision scattering models utilized in momentum-exchange (MEX) and symmetric charge-exchange (CEX) interactions. This juxtaposition is the result of the upgrade from a simple, isotropic scattering model to a differential cross-section-based, anisotropic scattering model which more accurately reflects true physics.

This paper will describe the numerical techniques used in the simulation, describe the details of the various scattering models as well as outline progress made on the models, and present the results of a comparison between simulation and experiment.

II. Numerical Tools & Domain

The simulation tool used in this study is MPIC.[1] MPIC is an axi-symmetric particle-based direct simulation Monte Carlo code capable of simulating nonequilibrium, rarefied flows with a PIC algorithm allowing for the calculation of electrostatic forces and an electron fluid solver. The PIC module determines the charge density at the nodes in the mesh based on the proximity of each particle to the surrounding nodes. The charge density is then used to compute the electric field at each node. This is accomplished either by incorporating the Boltzmann relation or solving for the potential directly using the detailed-fluid model, all while assuming quasi-neutrality. The potential is then differentiated spatially to obtain the electric fields. Subsequently, acceleration due to the electric field affects the trajectory of heavy species, though accelerations due to magnetic fields are ignored. MPIC utilizes a built-in DSMC algorithm and cross-section data for MEX and CEX, explained in more detail later, and is effectively parallelized.

The DSMC module handles collisions between the following heavy species: Xe and Xe^+ with the ability to handle Xe^{2+}, though unused in the present study. The DSMC method uses virtual particles to simulate collisions in rarefied gas flows. The particles represent real ions and neutrals and are grouped in cells whose characteristic lengths are shorter than a mean free path. Pairs of these particles are selected at random and a collision probability is evaluated that is proportional to the product of the relative velocity and collision cross-section. This probability is compared to a random number to determine if the collision occurs. If so, collision dynamics are performed to alter the properties of the colliding particles.

The experimental setup which is the focus of this simulation study is previously described by Wirz at UCLA[2] and consists of a 1500 V xenon ion beam being accelerated into a small, cylindrical facility held at a controlled pressure and temperature. The facility is converted into a numerically simplified axi-symmetric domain, seen in Figure 1. The domain, termed "the test cell", is 152 mm long and 48.24 mm in diameter with an inlet used for particle injection, an outlet for particle exit, and a line of rotation along the axis. As noted in the Figure, the two regions of particular interest are the inner cylinder (IC) and the exit plate (EP), representing regions where a direct comparison between simulation and experiment can be made. All walls and the inlet are defined by a Dirichlet boundary condition using a voltage of 0 V. The axis of rotation and outlet are defined by a Neumann boundary condition using a zero potential gradient. This numerical domain is held constant for all simulations, described later.

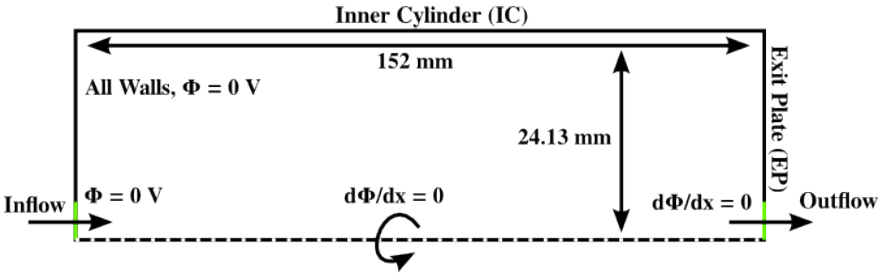

Figure 1. Numerical domain of the Wirz experiment, detailing inlet, outlet, and symmetry conditions as well as voltage conditions at the walls.

III. Scattering Models

The models used within MPIC for MEX and CEX interactions are between xenon neutral, Xe, and xenon ion, Xe^+ species. Firstly, for neutral-neutral collisions, the variable hard sphere model is employed[3] as follows:

$$\frac{\sigma_{MEX}}{\sigma_r} = \frac{g^{1-2\omega}}{g_r^{1-2\omega}} \tag{1}$$

Here, g_r is the relative collision speed at a reference temperature T_r and σ_r is the reference cross section based on a reference molecular diameter: $\sigma_r = \pi d_r^2$. Assuming $T_r = 273K$, ω and d_r values can be found for several major species in the literature.[3]

The models of interest to this study are 1) an isotropic scattering model which utilizes total cross-sections and 2) an anisotropic scattering model which utilizes differential cross-sections. Once a collision is determined to occur within MPIC, post-collision properties are calculated. Conservation of momentum and conservation of energy provide four out of the six equations required to calculate post-collision velocities. Typically, assumptions regarding the post-collision velocity direction, or scattering angle, are made to provide the remaining equations. In the present study, the MEX scattering angles are calculated by one of two methods: 1) isotropic scattering is assumed, or 2) anisotropic scattering based on later-mentioned semi-empirical differential cross sections is assumed. Method 1) treats the angular dependence of the colliding particles as unknown and assigns the direction of the post-collision relative velocity vector at random on a unit sphere. Method 2) is based on recent measurements of ion-atom differential cross-sections: these data are used to determine the post-collision in-plane relative velocity angles , whereas out-of-plane angles are chosen randomly. CEX collisions and their effects are modeled by creating an ion moving at the bulk velocity of neutrals at the original ion's location. The original ion is then removed from the list of ions and added to the list of neutrals. Scattering angles for CEX collisions are subsequently calculated corresponding to a simplistic analytic sampling distribution as described in the original development of MPIC.

The isotropic scattering model is presently used in MPIC and its original implementation is described in detail in the origins of the PIC module in MONACO. The isotropic scattering model utilizes total Xe-Xe^+ cross-sections calculated using the logarithmic formula proposed by Miller, et al.,[4] and the assumption that MEX and CEX cross sections are similar enough to be equated,[1,5]

$$\sigma_{\text{CEX}} = 171.23 - 27.2 \log g \ \text{Å}^2 \tag{2}$$

$$\sigma_{\text{MEX}} = \sigma_{CEX} \tag{3}$$

leading to a total cross section of $\sigma_{tot} = 44.1$ Å^2 for our particular study which contains an ion injection energy of 1500 eV, corresponding to a xenon ion velocity of 46,923 m/s.

MPIC has been upgraded to utilize differential cross-sections in the calculation of post-collision scattering angles, resulting in an anisotropic scattering process.[6] The differential cross-sections utilized are semi-empirical values experimentally verified at an interaction energy of 300 V.[7] Scharfe, et al., provide the following polynomial for calculating a curve-fit representative of differential cross-sections[8] in the laboratory frame,

$$\frac{d\sigma}{d\Omega}_{\text{LAB}} = \theta^{A_{el}} 10^{B_{el}} + (90-\theta)^{A_{ct}} 10^{B_{ct}}, \tag{4}$$

using the coefficients $A_{el} = -2.02$, $B_{el} = 3.24$, $A_{ct} = -1.098$, and $B_{ct} = -1.53$ to arrive at a bimodal distribution of differential cross-sections aimed at simulating MEX and CEX for a 300 eV interaction energy. This distribution is comprised of a MEX peak at low angles and CEX peak at high angles

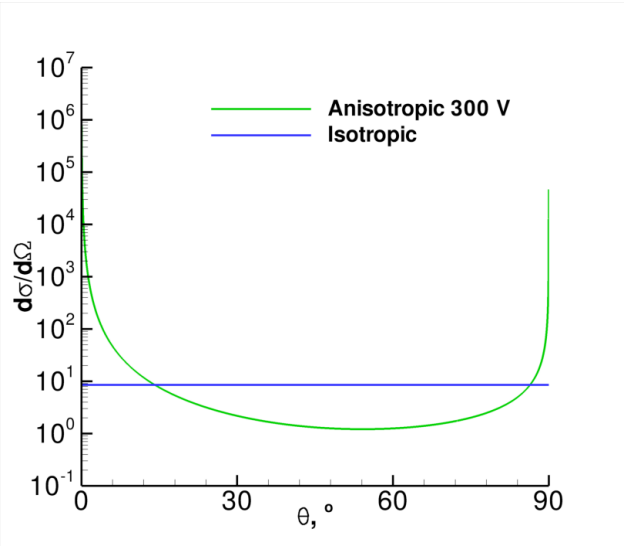

Figure 2. Differential cross section curve fits comparing the isotropic and 300 V anisotropic models in the laboratory frame.

Figure 2 shows the angular dependence of differential cross sections for the isotropic model and the anisotropic model in the laboratory frame calculated from Equation 4, displaying the constant probability of scattering angle for the isotropic model and the emphasis on very-low and very-high angles found in the anisotropic model. These low- and high-angle dependences portray the two dominant features of the Xe-Xe$^+$ interaction: MEX at low angles and CEX at high angles. It should be noted that the total cross-section for the anisotropic model is the same as that of the isotropic model; furthermore, the validity of the curve-fit found in Equation 4 can be tested by comparing Equation 2 with the integration of the differential cross-sections of Equation 4 as

$$\sigma_{\text{tot}} = \int_0^{\pi} \frac{d\sigma}{d\Omega}_{\text{LAB}} 2\pi \sin(\theta) d\theta, \tag{5}$$

while using the method of Scharfe et al. of applying constant $\frac{d\sigma}{d\Omega}_{\text{LAB}}$ within the very small and very large scattering angle values of $\frac{d\sigma}{d\Omega}_{\text{LAB}}$. The two critical angles within the range of the laboratory frame are θ_{el}, the location in the MEX peak where $\frac{d\sigma}{d\Omega}_{\text{LAB}}$ is constant starting from 0, and $\frac{\pi}{2} - \theta_{ct}$, the location in the CEX peak where $\frac{d\sigma}{d\Omega}_{\text{LAB}}$ is constant until $\frac{\pi}{2}$. Values of $\theta_{el} = 3.53 \times 10^{-5}$ degrees and $\theta_{ct} = 1.37 \times 10^{-3}$ degrees ensure that integration of the differential cross-section curve fit matches the total cross-section value. If these ranges of constant $\frac{d\sigma}{d\Omega}_{\text{LAB}}$ were not used, the differential cross-section curve-fit would asymptotically lead to extremely large values as Equation 4 approaches 0 and π.

One caveat of the semi-empirical curve-fit, however, is that it was fit to an experiment in which the xenon ion beam was accelerated to 300 V, corresponding to a total cross-section of 53.6 Å^2, not 1500 V, which corresponds to a total cross-section of 44.1 Å^2, as is characteristic of the UCLA experiment. Therefore, the same semi-empirical methodology as described by Chiu, et al.,[7] is applied to calculating differential cross-sections for 1500 V interactions leading to the following, refined coefficients, $A_{el} = -2.502$, $B_{el} = 3.508$, $A_{ct} = -1.380$, and $B_{ct} = -1.610$, using extreme-angle constant ranges of $\theta_{el} = 0.114$ degrees and $\theta_{ct} = 0.061$ degrees. This semi-empirical method of solving for interactions at different energies involves iteratively solving the equations for deflection angle, as laid out by Child,[9] using specific interaction potential models for xenon. The difference in these two differential cross-section models is shown in Figure 3. It can be seen that there is a lower magnitude "cross-section intensity" in the intermediate angles of the 1500 V interactions. Results will focus on comparing simulation techniques between MPIC isotropic and anisotropic models, low-energy and high-energy anisotropic models, and experiment.

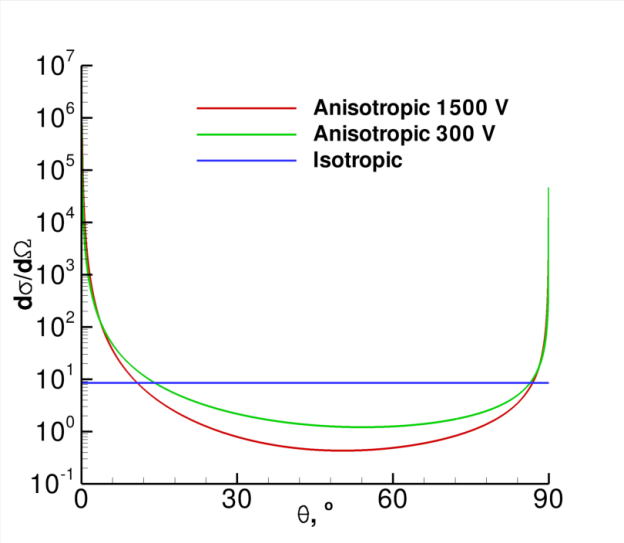

Figure 3. Differential cross section curve fits comparing the 300 V and 1500 V anisotropic models.

IV. Results

Numerical parameters are held constant throughout all simulations. Given an ion injection energy of 1500 eV, corresponding to a xenon ion velocity of 46,923 m/s, the time step is set to 1×10^{-8} s while the domain mesh is scaled using the relationship $v\,dt/dx = 0.3$ in order to arrive at an average mesh-edge length on the order of a millimeter, allowing for good resolution given the domain dimensions and fast particles. The test cell is first populated by neutral xenon species at a temperature of 298 K until the target background pressure is met and then is followed by the injection of the xenon ion beam at a total current of 29 nA. A list of background pressure values used can be found in Tables 1 and 2. Current density values are calculated by averaging density and velocity data after sampling for a large amount of time steps. This sampling method is also used to calculate current densities at the EP and IC through the averaging of particle fluxes onto the walls. Simulations required a total of 1,500,000 iterations with a total number of particles ranging from 700,000 particles for lower pressure solutions and 8,000,000 particles for higher pressure solutions. Total CPU time ranges from 136 hours for lower pressure solutions and 1,100 hours for higher pressure solutions with simulations running on a range of 16 to 40 CPU's depending on need.

Table 1. Current values for experimental results along the EP compared to the MPIC-isotropic model, MPIC-anisotropic model, and the refined MPIC-anisotropic model for 1500 V.

P (Torr)	UCLA-EP (nA)	Iso-EP	300V-EP	1500V-EP
2.0×10^{-6}	1.32	5.90	5.91	5.91
9.7×10^{-5}	1.36	5.16	5.55	5.16
2.49×10^{-4}	1.81	4.63	5.46	
4.98×10^{-4}	2.27	3.68	5.08	

Contour plots of current density for both isotropic and 300 V anisotropic MPIC results can be seen in Figure 4 for a medium-level pressure case of 4.96×10^{-4} Torr. Differences in the structure of the current density can be seen along the edges of the beam which suggest different scattering behavior. The isotropic model creates a larger footprint in the intermediate angles of scattering along the bulk of the beam while this footprint is not present in the anisotropic model results.

A comparison of collected currents at the inner cylinder (IC) and exit plate (EP) for isotropic, 300 V anisotropic, and experimental values at different operating background pressures and Knudsen number are

Table 2. Current values for experimental results at the IC compared to the MPIC-isotropic model, MPIC-anisotropic model, and the refined MPIC-anisotropic model for 1500 V.

P (Torr)	UCLA-IC (nA)	Iso-IC	300V-IC	1500V-IC
2.0×10^{-6}	0.0645	0.0995	0.0653	0.0556
9.7×10^{-5}	2.41	4.85	3.06	2.73
2.49×10^{-4}	5.16	10.8	7.19	
4.98×10^{-4}	8.01	17.6	12.7	

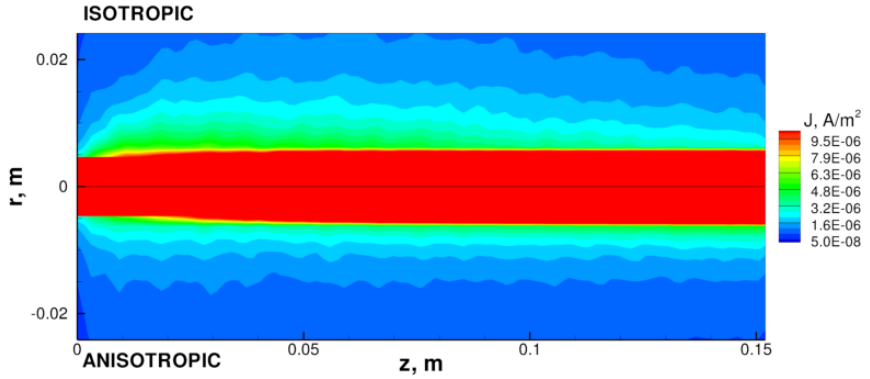

Figure 4. Contour plot of MPIC beam current density for isotropic (top) and 300 V anisotropic (bottom) models.

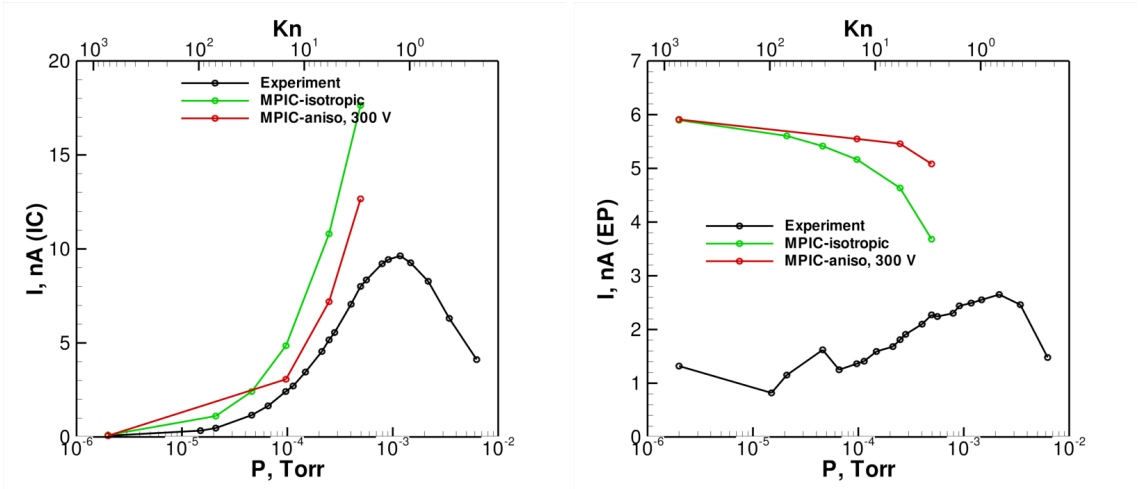

Figure 5. Current versus pressure results at the inner cylinder (IC, left) and exit plate (EP, right) of the test cell for two MPIC models and experiment.

shown in Figure 5. Current versus pressure trends match well for IC results and moderately well for EP results. Computed values of current collected for IC fall within 1% and 120% of measured results and computed values along the EP fall within 62% and 346% of experimental results. A complete list of current results is provided in Tables 1 and 2. The Knudsen number, defined as the ratio of the mean free path to characteristic length scale, $Kn = \lambda/L$, is calculated using the density of the background neutral xenon gas and the total cross-section for mean free path, $\lambda = 1/(\sqrt{2}\,\sigma\, n_n)$, and test cell diameter, $L = 48.26$ mm.

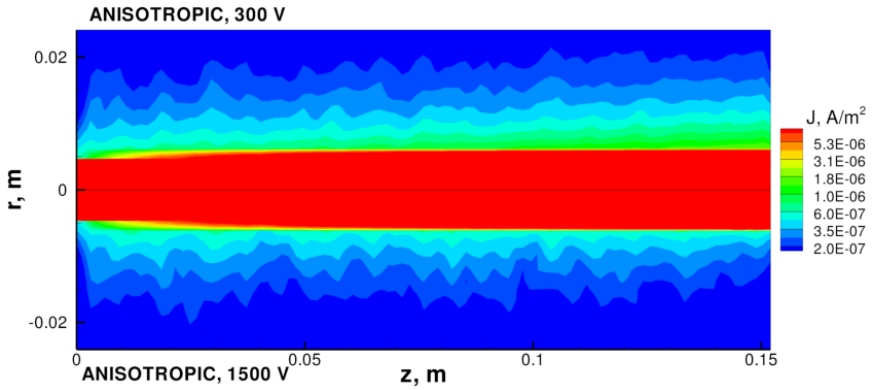

Figure 6. Contour plot of MPIC beam current density for the 300 V anisotropic model (top) and the 1500 V anisotropic model (bottom).

Contour plots of current density for the 300 V and refined, 1500 V anisotropic model MPIC results are shown in Figure 6 for a low-level pressure case of 9.75×10^{-5} Torr. Again, differences in the structure of the current density can be seen along the edges of the beam which suggest different scattering behaviors. The 300 V anisotropic model creates a slightly larger footprint in the low angles of scattering near the end of the beam while this footprint is not present, or is much smaller, in the 1500 V anisotropic model results.

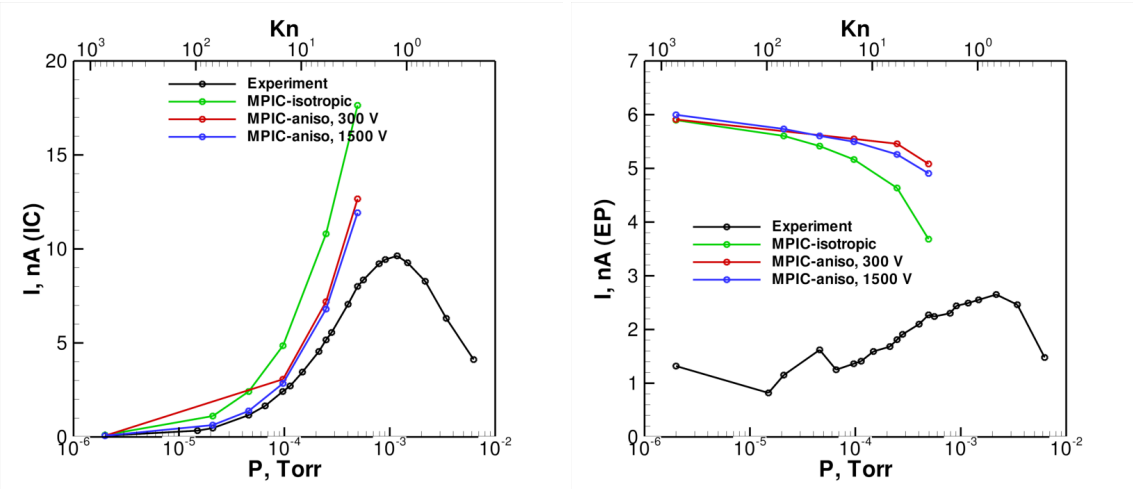

Figure 7. Current versus pressure results at the inner cylinder (IC, left) and exit plate (EP, right) of the test cell for all MPIC models and experiment.

A comparison of collected currents at the inner cylinder (IC) and exit plate (EP) for 300 V anisotropic and 1500 V anisotropic models at different operating background pressures and Knudsen number is included in Figure 7 alongside the experimental and isotropic data. Current versus pressure trends are closer to the measured data for IC and EP results for the refined 1500 V anisotropic model. Values for the refined anisotropic model can be seen in Tables 1 and 2 alongside the experiment and other model values.

V. Discussion

The contour comparisons of Figure 4 and the current versus pressure comparisons of Figure 5 are representative of the physical scattering differences between the isotropic and original 300 V anisotropic model. Due to fewer scattering events in the intermediate angles, the anisotropic model shows less current gathered at the IC of the domain. This additionally leads to more current collected at the EP as there is a shift to very small and very large angle interactions, representative of the shift in differential cross-sections as portrayed in Figure 2.

This is also true of the comparison between anisotropic models through the contour comparisons of Figure 6 and the current versus pressure comparisons of Figure 7. The refined 1500 V model accounts for even less intermediate angle scattering than the original 300 V model, pushing more scattering events to small and large angles, representative of the shift in differential cross-sections as portrayed in Figure 3.

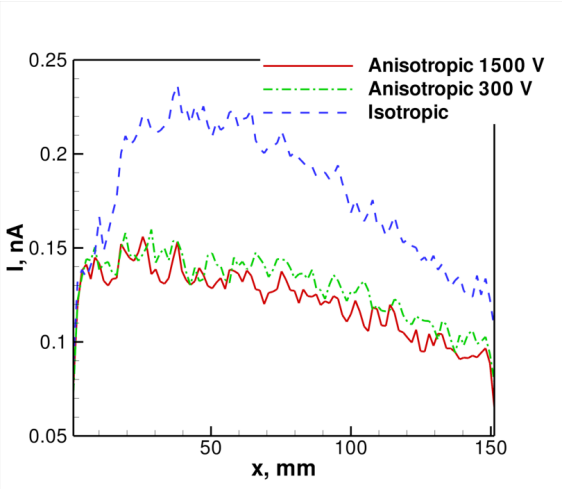

Figure 8. Spatial current results at the inner cylinder (IC) of the test cell for all models of MPIC.

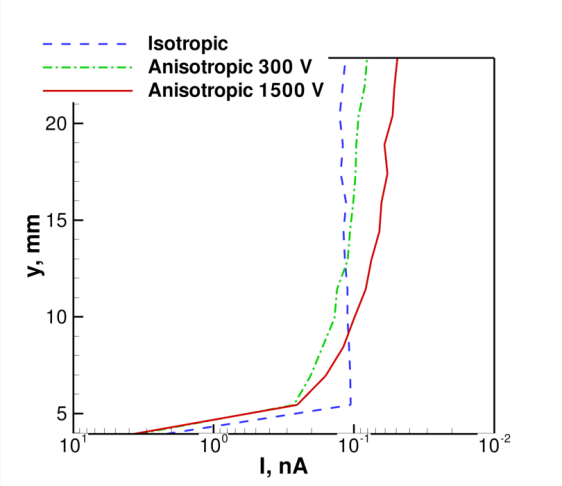

Figure 9. Spatial current results at the exit plate (EP) of the test cell for all models of MPIC.

This shift in scattering angles can be seen more clearly if a single pressure case is inspected spatially for current collected at specific locations along the EP and IC. While no experimental data exists for this observation yet, Figures 8 and 9 show IC and EP current collection, respectively, for the isotropic, anisotropic, and refined anisotropic models spatially for a higher pressure simulation of 4.96×10^{-4} Torr. Firstly, it can

be seen that the isotropic model shows significantly more current collection on both the EP and IC due to its uniformity of scattering angle selection; this is particularly true for the spatial EP figure in which current collection is constant. Secondly, the two anisotropic models show similar trends of spatial current collection in both EP and IC collection. The 1500 V anisotropic model, however, shows a current collection of slightly lower magnitude, though this lesser magnitude is more pronounced in the EP collection. These observations are again evidence of even less intermediate angle scattering events in the anisotropic models as compared to the isotropic model. In other words, more particles are remaining in the bulk of the beam and leaving the domain through the outlet rather than by impacting a wall.

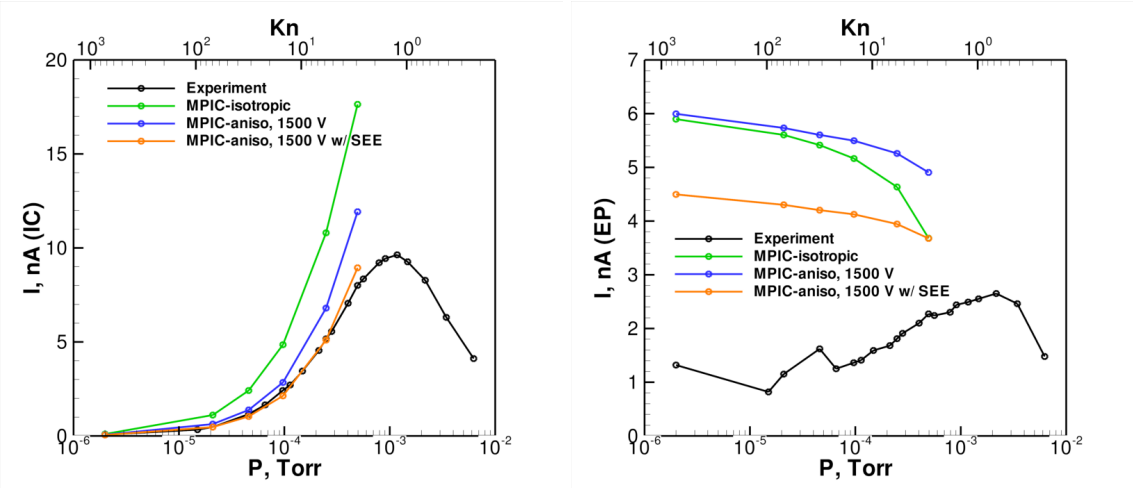

Figure 10. Current versus pressure results at the inner cylinder (IC, left) and exit plate (EP, right) of the test cell including an adjustment for secondary electron emission proportional to ion flux at the walls.

The lack of secondary electron emission (SEE) in the modeling could be argued as a large factor to explain the current discrepancies between experiment and simulation at the electrodes. In an environment with energetic particles such as this test cell, impacting (primary) heavy species can lead to the process of particle-induced emission of secondary electrons from the surface of the metal.[10] The classical description of SEE was proposed by Hobbs & Wesson[11] and relies on a coefficient, γ, which is the ratio of emitted electrons to primary impacting species, in terms of the fluxes of all species,

$$\Gamma_{se} = \frac{\gamma}{1-\gamma}\Gamma_{pi}, \tag{6}$$

with Γ_{se} representing the emitted secondary electron flux and Γ_{pi} representing the primary ion flux. For validation purposes, a constant secondary electron emission coefficient of $\gamma = 0.2$ is used which is typical of metals and allows for future comparison with other first-order models.[12] Ignoring the creation of secondary electrons due to high energy neutrals, a new value of current collection at the electrodes can be estimated by subtracting the current due to the flux of emitted electrons given by Equation 6 from the current due to impinging ion flux, the results of which are included in Figure 10. It can be seen that the subtraction of SEE current brings the values of collected current closer to experimental values. This correction is purely estimated but suggests the need for a higher fidelity SEE model for the purposes of comparing experiment to simulation.

Lastly, it should be stated that while the newly specified curve-fit coefficients create a differential cross-section model closer to reality and a current-collection trend closer to experiment, there is still a trend to overshoot the current at higher pressures and lower Knudsen numbers despite the addition of the SEE correction. It is in this region that the environment begins to crossover from a free-molecular to transitional regime and the importance of multi-collisional processes becomes present. With the chance that scattered ions are going through multiple interactions in order to reach the current-collecting walls of the test cell, there is the chance that many ions will not make it to the walls before being homogenized into the bulk environment. It remains to be seen if future MPIC simulations conducted at higher pressures will successfully predict this trend.

VI. Conclusion

The comparison of isotropic and anisotropic MEX and CEX scattering models using MPIC has advanced the fidelity of the current simulation effort for analysis of the experimental data from the UCLA test cell. The addition and refinement of the anisotropic cross-section and scattering algorithms has led to the closest agreement for integrated currents between simulation and experimental data supplied at the specified locations of IC and EP. These results represent an increase in fidelity of the heavy species interaction models used in this tool. Additionally, simulated spatial current data can be compared to future experimentally gathered current via the construction of segmented collectors at the walls of the IC. Lastly, the addition of a rudimentary SEE correction illustrates the need for even higher fidelity models for the purpose of reaching improved agreement with experiment.

Acknowledgments

The authors would like to thank Tyler Huismann of the Nonequilibrium Gas and Plasma Dynamics Laboratory, Richard Wirz at UCLA, Spencer Olson and Nate Lockwood at Kirtland AFB, Justin Koo and Michelle Scharfe at Edwards AFB, and Rainer Dressler at Spectral Sciences. This work was supported by the University of Michigan/AFRL Center of Excellence in Electric Propulsion (MACEEP), Grant #F9550-09-1-0695.

References

[1]Y. Choi. *Modeling an anode layer Hall thruster and its plume*. Phd dissertation, University of Michigan, 2008.

[2]R. Wirz, L. Chu, M. Patino, H. Mao, and S. Araki. Well-Characterized Plasma Experiments for Validation of Computational Models. In *32nd International Electric Propulsion Conference*, pages IEPC–2011–122, Wiesbaden, Germany, 2011.

[3]G. A. Bird. *Molecular gas dynamics and the direct simulation of gas flows*. Clarendon, 1994.

[4]J. S. Miller, S. H. Pullins, D. J. Levandier, Y. Chiu, and R. A. Dressler. Xenon charge exchange cross sections for electrostatic thruster models. *Journal of Applied Physics*, 91(3):984–991, 2002.

[5]C. Cai. *Theoretical and Numerical Studies of Plume Flows in Vacuum Chambers*. Phd dissertation, University of Michigan, 2005.

[6]T. D. Huismann and I. D. Boyd. Improving Hall-thruster Plume Simulation through Investigation of the Near-field Environment. In *International Electric Propulsion Conference*, pages IEPC–2011–227, Wiesbaden, Germany, 2011.

[7]R. A. Dressler, Y. Chiu, D. J. Levandier, C. Houchins, and C. Y. Ng. Large-Angle Xenon Ion Scattering in Xe-Propelled Electrostatic Thrusters: Differential Cross Sections. *Journal of Physics D: Applied Physics*, 41(16):165503, August 2008.

[8]M. K. Scharfe, J. W. Koo, and G. M. Azarnia. DSMC Implementation of Experimentally-Based Xe++ Xe Differential Cross Sections for Electric Propulsion Modeling. In *27th International Symposium on Rarefied Gas Dynamics*, number 10271. DTIC Document, 2011.

[9]M. S. Child. *Molecular Collision Theory*. Academic Press, 1974.

[10]P. Varga and H. Winter. Slow Particle-Induced Electron Emission from Solid Surfaces. In *Particle Induced Electron Emission II*, pages 149–213. 1992.

[11]G.D. Hobbs and J.A. Wesson. Heat flow through a Langmuir sheath in the presence of electron emission. *Plasma Physics*, 9(1):85–87, January 1967.

[12]S. J. Araki and R. E. Wirz. Collision Modeling for High Velocity Ions in a Quiescent Gas. In *42nd AIAA Plasmadynamics and Lasers Conference*, pages AIAA 2011–3740, Honolulu, HI, 2011.